Spectrochimica Acta Part A: Molecular and Biomolecular Spectroscopy 292 (2023) 122409

Contents lists available at ScienceDirect

Spectrochimica Acta Part A: Molecular and Biomolecular Spectroscopy

journal homepage: www.journals.elsevier.com/spectrochimica-acta-part-a-molecular-and-biomolecular-spectroscopy

Differentiation of blood and environmental interfering stains on substrates by Chemometrics-Assisted ATR FTIR spectroscopy

Cristina Cano-Trujillo [a,b], Carmen García-Ruiz [a,b], Fernando E. Ortega-Ojeda [a,b,c], Gemma Montalvo [a,b,*]

[a] Universidad de Alcalá, Departamento de Química Analítica, Química Física e Ingeniería Química, Ctra. Madrid-Barcelona km 33,6, 28871 Alcalá de Henares, Madrid, España

[b] Universidad de Alcalá, Instituto Universitario de Investigación en Ciencias Policiales (IUICP), Calle Libreros 27, 28801 Alcalá de Henares, Madrid, España

[c] Universidad de Alcalá, Departamento de Ciencias de la Computación, Ctra. Madrid-Barcelona km 33,6, 28871 Alcalá de Henares, Madrid, España

HIGHLIGHTS

- Bloodstains can be identified independently of the substrate they are on.
- Bloodstains can be differentiated from three interferents.
- ATR FTIR spectroscopy and chemometrics show a high potential in forensics.

GRAPHICAL ABSTRACT

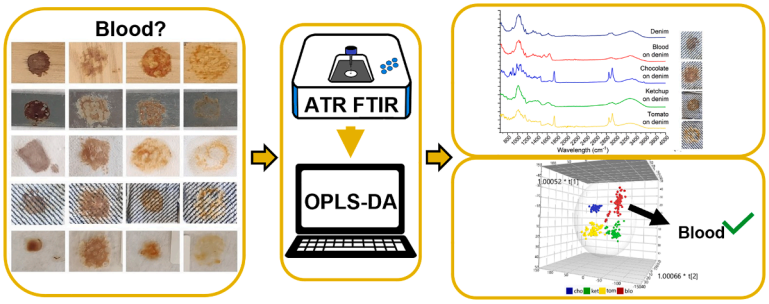

ARTICLE INFO

Keywords:
Blood
Interferent
Substrate
Vibrational spectroscopy
ATR FTIR
OPLS-DA

ABSTRACT

Blood is the most common and relevant bodily fluid that can be found in crime scenes. It is critical to correctly identify it, and to be able to differentiate it from other substances that may also appear at the crime scene. In this work, several stains of blood, chocolate, ketchup, and tomato sauce on five different substrates (plywood, metal, gauze, denim, and glass) were analysed by ATR FTIR spectroscopy assisted with orthogonal partial least square-discriminant analysis (OPLS-DA) models. It was possible to differentiate blood from the environmental interfering substances independently of the substrate they were on, and to differentiate bloodstains according to the substrate they were deposited on. These results represent a proof-of-concept that open new horizons to differentiate bloodstains from other interfering substances on common substrates present in crime scenes.

Abbreviations: ATR, attenuated total reflectance; AUC, area under the curve; FPR, false positive classification rate; LDA, linear discriminant analysis; OPLS-DA, orthogonal partial least squares discriminant analysis; PCA, principal component analysis; PCs, principal components; PLS, partial least squares; PLS-DA, partial least square discriminant analysis; PLSR, partial least square regression; ROC, receiver operating characteristic; SIMCA, soft independent modelling of class analogy; SNV, standard normal variate; TPR, true positive classification rate; VIP, variable of importance for the model.

* Corresponding author at: Universidad de Alcalá, Departamento de Química Analítica, Química Física e Ingeniería Química, Ctra. Madrid-Barcelona km 33,6, 28871 Alcalá de Henares, Madrid, España.

E-mail address: gemma.montalvo@uah.es (G. Montalvo).

https://doi.org/10.1016/j.saa.2023.122409
Received 25 July 2022; Received in revised form 23 December 2022; Accepted 23 January 2023
Available online 26 January 2023

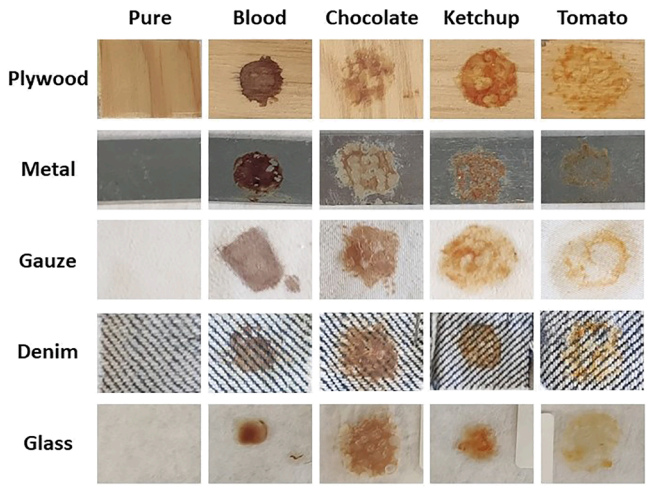

Fig. 1. Photographs of the dried stains of blood, chocolate, ketchup, and tomato sauce on the five different substrates employed: plywood, metal, gauze, denim, and glass. Photographs of the substrates without stains are also included.

1. Introduction

When a crime is committed, different traces can be found at the crime scene. Bodily fluids are of extremely relevance due to the amount of information they can provide to criminal investigators. Within the bodily fluids, blood is the most important one. Bloodstains are usually found in violent crimes, such as murder, robbery, battery, sexual assaults, etc. Analysing the bloodstains allow the investigators to determine what kind of crime was committed, which weapon was used, if the blood is human or from an animal, if it is relevant to the case or not, if blood is mixed with other bodily fluids, etc [1,2]. There may also be substances that resemble bloodstains or that could give false positives on a detection test at the crime scene. These are called environmental interferences [3].

For all of this, the identification of the stains like blood and its differentiation from other bodily fluids or artificial substances is imperative. Bloodstains have been traditionally analysed by presumptive tests, like luminol or leucomalachite green, and confirmatory techniques such as immunochromatographic techniques, which are destructive to the sample [3], time-consuming [2], and not so simple. For crime scene investigations, it is paramount that the samples are identified as soon as possible and preserved for further analysis in the laboratory. The amount of blood found at the scene may be very small and necessary for subsequent DNA extraction, so destruction of the sample in the identification process should be avoided. Moreover, traditional tests are not able to detect mixed stains [4].

These reasons explain why the scientific community is looking for non-destructive, simple, selective, and fast techniques to analyse bloodstains, such as attenuated total reflectance Fourier transform infrared spectroscopy (ATR FTIR). This technique is based on the measurement of the changes that occur in the dipole moment of bonds after an excitation with electromagnetic radiation [2]. The FTIR spectrum depends on the chemical composition [5]. When two substances have a different chemical composition, their spectra will also be different. Hence, when the same substance changes its composition (for example, during blood ageing), so does its spectrum. Therefore, the technique can be used to differentiate substances from each other [5–12], as well as to monitor changes in a substance over time [4,10]. The first portable ATR FTIR was developed by Agilent Technologies in 2008. Since then, the spectrometer has been used to analyse composites, polymers, coatings, and contaminants in the automobile, metal, biomedical, electronics industry [13], etc. With them, ATR FTIR could also be used *in situ* at the crime scene [5,12,13].

The data obtained from ATR FTIR is large and complex and must be processed (cleansed and filtered) mathematically using chemometrics. The literature collects interesting studies regarding ATR FTIR's application on different biological fluids. Zapata *et al.* used ATR FTIR with principal component analysis (PCA) and soft independent modelling of class analogy (SIMCA) to distinguish semen, vaginal fluid, and urine from each other and non-bodily fluid substances on different substrates. They also successfully studied semen-vaginal fluid mixtures [7].

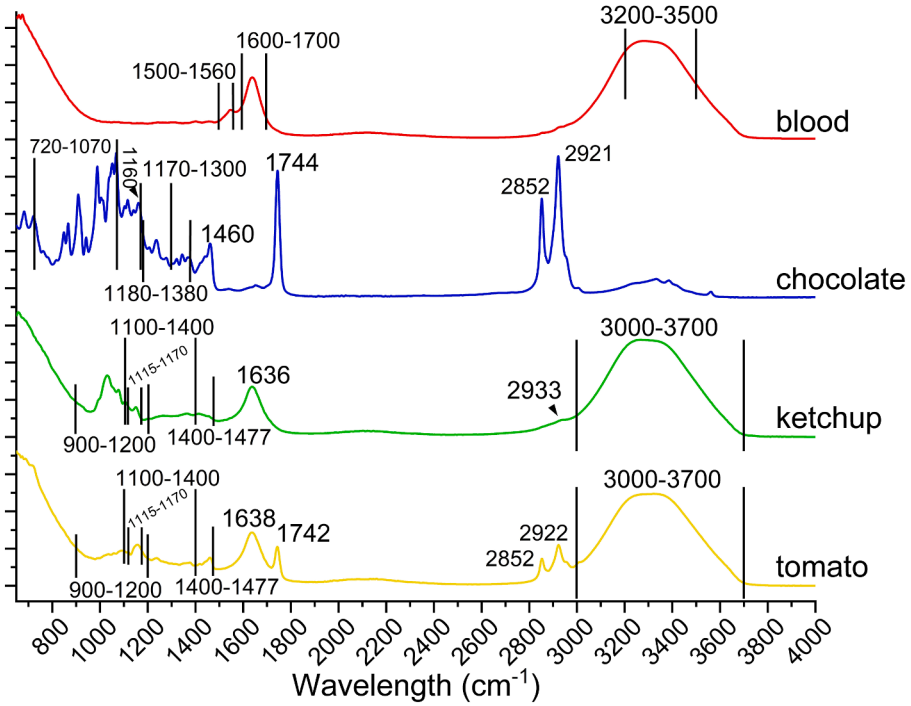

Fig. 2. Average ATR FTIR spectra of blood, chocolate, ketchup, and tomato sauce measured directly on the diamond crystal, immediately after the deposition. The main fluids' bands are marked in their corresponding spectra.

Table 1
Characteristic bands of the fluids analysed by ATR FTIR and their corresponding functional groups.

Substance	Wavelength (cm^{-1})	Vibrational mode	Main attribution	Reference
Blood	698	Amide IV (C—H bending)	Protein	[12]
	1560–1500	Amide II (N—H bending and C—N stretching)		
	1600–1700	Amide I (C═O stretching)		
	3200–3500	O—H stretching	Hydroxyl in water	
Chocolate	720	CH_2 rocking	Tryacilglycerols	[17]
	848			
	865			
	908			
	988			
	1067			
	1160	C—O stretching	Tryacilglycerols in liquid state	
	1236	CH_2 wagging CH_2 twisting	Tryacilglycerols	
	1363	CH_2 wagging		
	1460	CH_2 scissoring		
	1744	C═O stretching	Glycerol backbone's disordered conformational state	
	2852	C—H symmetric stretching	Polymethylene segments	
	2921	C—H asymmetric stretching		
Ketchup	1030	C—O—C	Carbohydrates and acids	[18]
	1077			
	1105	C—C stretching C—C—H stretching C—O—C[1]	[1]Carbohydrates and acids	[18,20]
	1151	C—C stretching C—C—H stretching C—O stretching C—O—C[1]		
	1416	C—H bending		[18]
	1459	CH_2	Trans-lycopene	[19]
	1636	C═C stretching	Olefin	[19,20]
	2933	Asymmetrical CH_2	Lipids	[19]
	3303	O—H stretching	Water bands	[18]
Tomato	1096	C—O—C	Carbohydrates and acids	[18]
	1158	C—C stretching C—C—H stretching C—O stretching C—O—C[1]	[1]Carbohydrates and acids	[18,20]
	1235	C—C stretching		
	1378	C—C—H stretching		[18]
	1460	C—H bending CH_2	Trans-lycopene	[18–20]
	1638	C═C stretching	Olefin	[19,20]
	1742		Lipids	[18]
	2852	[2]Methylene C—H asymmetric stretching	[2]Lycopene	[18–20]
	2922	[2]Methylene C—H		
	3347	symmetric stretching O—H stretching	Water bands	[18]

Takamura *et al.,* in 2017, differentiated *antemortem* and *postmortem* blood on different substrates by ATR FTIR and a partial least square discriminant analysis (PLS-DA) [9]. Also, in 2018, they differentiated peripheral blood, saliva, semen, urine, and sweat by ATR FTIR spectroscopy and chemometrics, and those bodily fluids from non-bodily fluid substances. They also studied sample-aging [10]. Kumar *et al.* studied bloodstains aging by ATR FTIR and chemometrics [4]. Mistek-Morabito *et al.* employed ATR FTIR and PLS-DA to differentiate between human and animal blood [12], while in 2021 they combined ATR FTIR with PCA and PLS-DA to discriminate peripheral blood, menstrual blood, and vaginal fluid [5]. In 2020, Sharma *et al.* used ATR FTIR along with PCA, linear discriminant analysis (LDA) and partial least square regression (PLSR) to differentiate menstrual blood from peripheral blood, seminal and vaginal fluid. Although only menstrual blood was measured as stains on different substrates, menstrual blood, and the other fluids (including the non-bodily fluids) were deposited on glass and, once they were dried, they were scraped out and placed on the ATR's diamond crystal [11].

Bloodstains can be found on a wide range of different surfaces, both porous and non-porous materials. When blood is in a porous substrate, it tends to get through the layers of the material until it dries; by contrast, when blood is on a non-porous substrate, it accumulates and dries on the surface [1]. This is important, because the intensity of the bands in the infrared (IR) spectrum can be weaker or overlapping when the fluids are in porous substrates [8].

The main objective of this investigation is to identify bloodstains on five different substrates: plywood, metal, gauze, denim, and glass. Those are surfaces usually present in crime scenes. A second objective was the differentiation of bloodstains from three environmental interferent stains that could be confused with blood: chocolate, ketchup, and tomato sauce. To achieve these objectives, ATR FTIR was employed to analyse the bloodstains and the interferents stains on the five different substrates. The data obtained was used to create orthogonal partial least square-discriminant analysis (OPLS-DA) models.

2. Materials and methods

2.1. Samples

Human blood was obtained from one female donor by pricking the index finger with a lancet. Interferents may be commonly found as environmental interfering stains in a crime scene. In this study, chocolate, tomato sauce, and ketchup were used as interferents. Chocolate (milk chocolate, Mr. Wonderful, Spain) was composed of sugar, cocoa butter, cocoa mass, milk powder, emulsifier, and flavourings; ketchup (Heinz, Pittsburgh, Pennsylvania, United States), and tomato sauce (Solís, Nestlé, Vevey, Switzerland) were bought from a local supermarket. Both fluids were composed by tomato, sugar, salt, and species. The ketchup also had alcohol vinegar and celery in its ingredients, which are not present in the tomato sauce. The tomato sauce also had sunflower oil, corn starch, and onion.

Five common (everywhere) substrates were used as substrates: wood (plywood), metal (galvanised iron), gauze (white polyester), denim (100 % cotton blue denim), and glass (glass slide). All the substrates were cut in 4x4 cm pieces. They were also analysed to obtain a reference background.

A blood drop (after pricking a finger of the donor) was placed

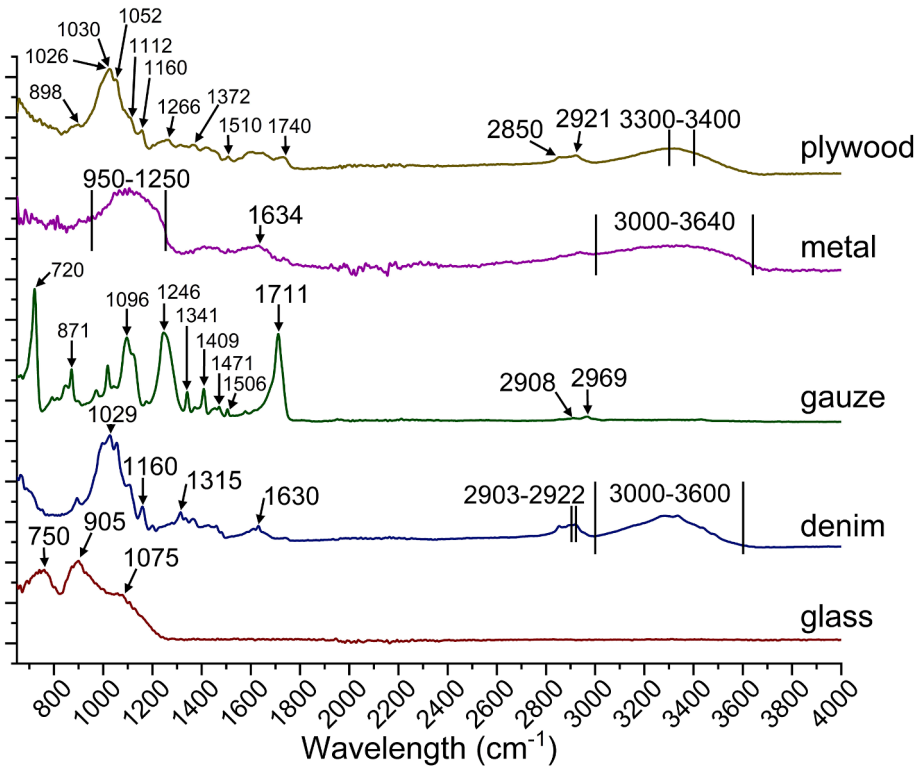

Fig. 3. Average ATR FTIR spectra of the pure substrates. The figure shows the main bands of each substrate.

directly on the substrates, by simple deposition, and left to dry at ambient conditions. This procedure was made to mimic the conditions that would be found at a crime scene and no bloodstain segregation was observed visually. A small amount of the interfering substance, like the tip of a spatula, was placed on the same type of substrates as the blood. All the fluids (blood and environmental interferents) were also placed directly on the diamond crystal of the FTIR to measure their pure spectra. 24 stains were measured: Four of them were directly deposited on the diamond crystal; and 20 different stains were deposited on substrates (four substances on five different substrates).

2.2. Instrumentation

The measurements were made with a Nicolet iS10 FTIR Spectrometer (Thermo Fisher Scientific, Waltham, Massachusetts, United States) and the Smart Orbit iTR ATR with a diamond crystal component equipped with the OMNIC software (Thermo Fisher Scientific, Waltham, Massachusetts, United States). The Smart Orbit ATR accessory works in single-reflection. The absorption-mode spectra were recorded in the 500 to 4000 cm^{-1} range with a resolution of 8 cm^{-1} with 32 scans. The background (air) was measured before analysing each sample, approximately every 10 min.

Each sample, placed directly on the diamond crystal of the ATR-spectrometer (pure blood and different substances) or on the substrates, was measured ten times. When analysing the stains on the substrates, five spectra were obtained from the outer part and other five spectra from the inner part of the studied spots. The spectra showed in the figures are the averaged signal of the different spectra collected. The diamond crystal of the spectrometer was cleaned with propanol between the measurements of the different fluids and substrates.

2.3. Data treatment

All the spectra were imported and organised into a Microsoft Excel v2008 (Microsoft Corporation, Redmond, Washington, United States) matrix. Then, this matrix was imported into The Unscrambler X 10.4 version (CAMO-Aspen Technology, Houston, United States) for the data pre-processing. The pre-processing step is important to further cleanse the data, reduce its abnormal variation, scatter effects, and random noise [14]. This in-chain mathematical treatment included the typical spectral data pre-processing: A baseline offset, standard normal variate (SNV) normalisation, and the Savitzky-Golay smoothing (2nd order polynomial and 7 smoothing points). The cleaned data was then imported into SIMCA v17.02 (Sartorius, Göttingen, Germany) for modelling.

A Principal Component Analysis (PCA) was carried out to explore the data. PCA is a multivariate projection method that reduces the dimension of the data facilitating the overview of the multivariate data. PCA makes it possible to find which data objects (individuals) group together and which do not fit the model (outliers) [15]. In addition, orthogonal partial least squares-discriminant analysis (OPLS-DA) models were created to differentiate bloodstains on the different substrates (plywood, metal, gauze, denim, and glass). OPLS-DA was also used to try differentiating among blood and the environmental interfering stains independently of the substrate where they were deposited on. OPLS is a modification of partial least squares (PLS) in which the variation in the X-matrix is divided: one part is related to the Y-matrix and the other part is not related to the Y-matrix, which is the orthogonal part [15]. In an OPLS-DA model, a component acts as a predictor of a class, while the remaining components of the model explain the variability orthogonal to the predictor. In this study, the OPLS-DA models were made using cross validation with the leave-one-out method. For this purpose, the sample set was automatically divided into seven groups. For each validation, one of the seven groups was taken as a test set and the remaining six groups as a whole training set. For the next validation, the group previously used as test set was returned to the training set, and the second group of samples were excluded and used as a test set. In this way, each of the seven groups was tested once, allowing the best performing model to be obtained without reaching under- or over-fitting conditions. In OPLS-DA, there are two key terms that allow us to

Table 2
Characteristic bands of the substrates measured by ATR FTIR.

Surface	Wavelength (cm^{-1})	Vibrational mode	Main attribution	Reference
Plywood	898	Glucose ring stretching C_1-H deformation	Cellulose	[21]
	~1026	C—O of primary alcohol Guaiacyl C—H	Lignin	
	1030 1052	C—O stretching	Cellulose	
	1112	Asymmetric glucose ring stretching		
	~1160	C—O—C asymmetric vibration		
	1266	C—O of guaiacyl ring	Lignin	
	1372	C—H symmetric deformation	Cellulose	
	1510	C═C	Lignin	
	1740	C═O	Cellulose	
	2850 2921	C—H stretching	Lignin	
	3300–3400	O—H stretching	Cellulose Lignin	
Metal	950–1250	PO_4^{3-}	Phosphates from the coating	[23]
	1634	O—H bending	Hydration water of the coating	
	3000–3640	O—H stretching		
Gauze	720	C—H bending, C—H rocking in C-CH_2-		[24]
	871	Aromatic ring C—H bending		
	1096	C—O stretching		
	1246	C—O stretching	Ester groups	
	1341 1409 1471	C—H bending		
	1506	Aromatic ring C═C stretching		
	1711	C═O stretching	Polyester	
	2908 2969	C—H stretching		
Denim	1000–1200	Cellulose bands	Cellulose in cotton	[25]
	1029	C—O stretching	Cellulose	
	1160	C—O—C stretching		
	1315	C—H wagging		
	1630	O—H bending	Absorbed water	
	2903–2922	Aliphatic C—H stretching	Waxes	
	3000–3600	N—H stretching O—H stretching	Water bands Dye molecules Glucose	
Glass	750	Si-O$^-$ symmetric stretching	Si_2O	[26]
	905	Si-O$^-$ asymmetric stretching		
	1075	Si-O-Si asymmetric stretching		

interpret the model with a high goodness of fitting: R^2X and Q^2X. While R^2X indicates the amount of variation of a variable that is explained by the model, Q^2X is the cross-validated version of R^2X, which determines the predictive ability of the model. When both values are greater than 0.5, the model could be considered as robust and having a good predictive ability. The confidence level of the parameters and the significance level for the Hotelling's T^2 were set to 95 % and 0.05, respectively [16]. The Hotelling's T^2 plot represented the distance to the centre of the model for each sample, acting as a multivariate equivalent of the well-known *t*-student parameter. In this plot, two confidence limits (95 and 99 %) were stablished. If the T^2 value of one sample was larger than the 99 % limit, that observation was considered an outlier that could negatively affect the model. Instead of using the traditional loadings plots, less practical when representing hundreds of wavelengths, the contribution, or the variable of importance for the model (VIP) plots were used to determine which of the variables had the greatest influence on the outcome of the model. The receiver operating characteristic (ROC) plot showed how good was the performance of the classification/discrimination model. In this plot, the true positive classification rate (TPR) was plotted in the Y-axis, while the false positive classification rate (FPR) was represented in the X-axis. How well the model classified the samples was quantitatively tested by the area under the curve (AUC). If the value was close to 0.5, the model performed bad classifications, while values close to 1 indicated nearly a perfect classification.

The same matrix used to build the OPLS-DA models was used to create the graphics, which were made with ORIGIN v2021 (OriginLab, Northampton, Massachusetts, United States).

3. Results and discussion

3.1. IR spectral characterization of blood from environmental interfering stains

There are some common substances that may form part of a stain and could act as environmental interferents of bloodstains present at a crime scene. Fig. 1 shows blood and some common interfering stains (chocolate, ketchup, or tomato sauce) on several substrates (plywood, metal, gauze, denim, and glass).

Fig. 2 shows the spectra of blood, chocolate, ketchup, and tomato sauce obtained by ATR FTIR measured directly on the diamond crystal, immediately after their deposition. The spectra of these four fresh samples are different, although some bands are common in all of them. Table 1 summarises the characteristic bands of all the studied fluids. In the blood spectra, the 3200–3500 cm^{-1} region was intense and corresponds mainly to the O—H stretching of the samples' water [12]. In the same region appeared the vibration band of the N—H stretching from the amides. By contrast, the 2852 cm^{-1} and 2921 cm^{-1} bands (which correspond to the symmetric and asymmetric CH_3 stretching) [5,12] were not prominent in the blood spectrum. The 1600–1700 cm^{-1} (which corresponds to the Amide I C═O stretching vibrations) and the 1500–1560 cm^{-1} (which correspond to Amide II N—H bending vibrations) regions could be used to differentiate blood from the three environmental interferents. The bands located at 1390 cm^{-1} (CH_3 symmetric bending), 1239 cm^{-1} (Amide III, coupled C—N stretching and N—H bend vibrations) and 1082 cm^{-1} (glucose) were not seen in this blood spectra [5,12].

The chocolate spectrum showed two very pronounced bands at 2852 cm^{-1} and 2921 cm^{-1}, which correlates with the symmetric and antisymmetric CH_2 stretching modes of the acyl chains. The band at 720 cm^{-1} correspond to the CH_2 rocking mode, whilst the band at 1460 cm^{-1} can be attributed to a CH_2 scissoring in the polymethylene segments. The 1180–1380 cm^{-1} region showed different bands that correspond to the tryacilglycerols CH_2 wagging. The 720–1070 cm^{-1} region correlates to the CH_2 rocking modes, and the 1170–1300 cm^{-1} region corresponds to the CH_2 twisting. The tryacilglycerols C—O stretching mode in liquid state could be responsible for the band at 1160 cm^{-1}. The band at 1744 cm^{-1} is related to the C═O stretching from the glycerol backbone's disordered conformational state [17].

The ketchup and tomato sauce spectra showed some similar bands, while there were other bands that allowed for their differentiation. This can be explained by their similar composition because both fluids are

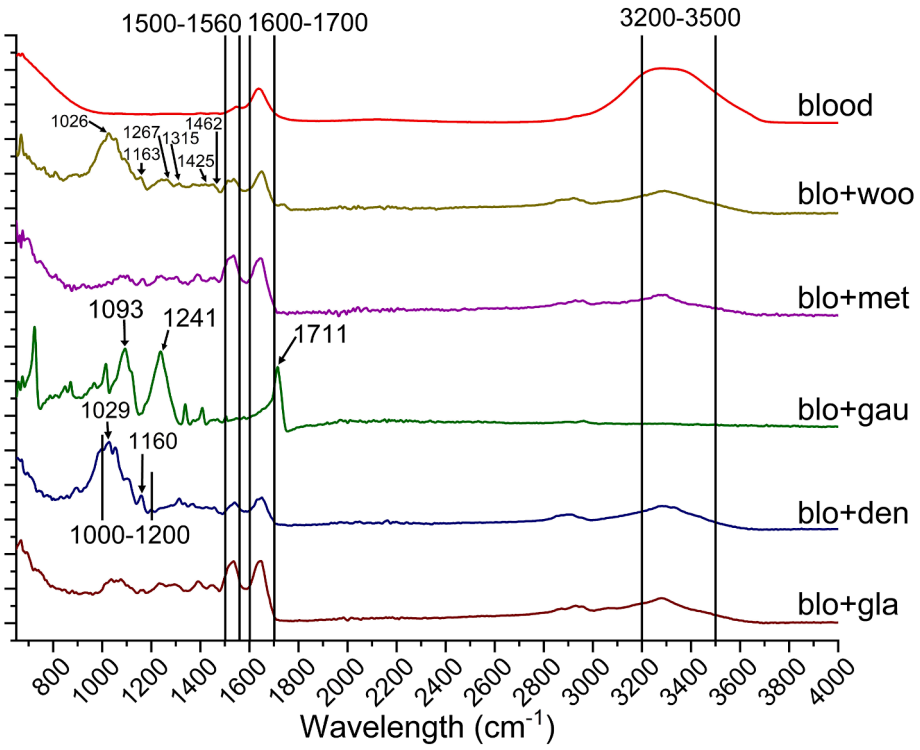

Fig. 4. Average ATR FTIR spectra of bloodstains on different substrates. The figure shows the blood's and substrates' characteristic bands.

composed by tomato, sugar, salt, and species. Additional ingredients are given in the experimental section. The band at 1636 cm^{-1} in the ketchup spectra and the band at 1638 cm^{-1} in the tomato sauce spectra are related to an amide group [18]. They are also related to an overlapping by the lycopene C═C stretching band [19]. The lipid-related bands are located between 1730 and 1765 cm^{-1} and 2800–3000 cm^{-1} [18], which can be seen in the tomato sauce but not in the ketchup spectra. Specifically, the 2922 cm^{-1} and 2852 cm^{-1} bands found in the tomato sauce spectra are related to the lycopene's C—H symmetric and asymmetric stretching [19]. The 2933 cm^{-1} band in the ketchup spectra could be due to an asymmetrical CH_2 group that is related to a 2929 cm^{-1} band according to the literature [19]. The C—H bending appeared at 1400–1477 cm^{-1}, the C—C and C—C—H stretching at 1100–1400 cm^{-1}, and the C—O stretching at 1115–1170 cm^{-1} [18]. The bands from these functional groups can be seen both in the ketchup and tomato sauce spectra. The bands attributed to the *trans*-lycopene CH_2 at 1458–1465 cm^{-1} can be observed in both spectra [19]. The water bands located at 3000–3700 cm^{-1}, and the carbohydrates and acids vibrational modes (C—O—C) bands located at 900–1200 cm^{-1} can also be seen in both spectra [18].

3.2. IR spectral characterization of the substrates

Five different substrates were employed to make the stains: wood (plywood), metal (galvanised iron), gauze (white polyester), denim (100 % cotton blue denim), and glass (glass slide). These kinds of materials were selected because they can be easily found at the crime scene. Therefore, the stains of biological fluids may be found on these surfaces and may represent real-life situations in forensic investigations, allowing its application on real investigations of a crime scene. Fig. 3 shows the pure spectra of those substrates, whilst Table 2 shows their characteristic bands as well as their detailed attribution with the corresponding vibrational modes and the assignment with the related component. The plywood spectrum, as expected, was dominated by the lignin and cellulose bands, since these two polymers are fundamental components of wood. The bands at 1030 cm^{-1} and 1052 cm^{-1}, corresponding to a cellulose C—O stretching, were the most intense bands in the spectrum. The 1200–1740 cm^{-1} range showed many bands from the different vibrational modes of cellulose and lignin. Another two regions were highlighted in the spectrum: The lignin C—H stretching bands at 2921 and 2850 cm^{-1}, and the 3300–3400 cm^{-1} region related to the cellulose and lignin O—H stretching [21].

The metal sample was galvanised steel. The galvanizing process protects steel from corrosion by creating a zinc coating [22]. The spectrum had a broad band in the 950–1250 cm^{-1} region, which could probably correspond to the phosphate groups (PO_4^{3-}) from the zinc phosphate coating. Usually, this coating is composed by crystalline α-hopeite, orthorhombic α-$[Zn_3(PO_4)_2{\cdot}4H_2O]$, and crystalline phosphophyllite $[Zn_2Fe(PO_4)_2{\cdot}4H_2O]$. The wide 3000 to 3640 cm^{-1} region is due to the O—H stretching, while the water bending vibrations can be observed in the band at 1634 cm^{-1} [23].

The gauze is mainly composed by polyester. Four bands in the gauze spectrum stand out from the others. These bands are the C—H bending at 720 cm^{-1}, C—O stretching at 1096 cm^{-1}, the ester groups C—O stretching at 1246 cm^{-1}, and the polyester C═O stretching at 1711 cm^{-1} [24].

The composition of denim is 100 % blue cotton. In the denim spectra, the region between 1000 and 1200 cm^{-1}, which correspond to cellulose bands from cotton, is the most intense of the spectrum. Due to the presence of cellulose in denim, some similarities exist between the wood and the denim in that region of the spectra. The aliphatic C—H stretching from waxes located in the 2903–2922 cm^{-1} range is also highlighted, along the 3000–3600 cm^{-1} region, which is known to show the dye molecules N—H stretching and the glucose alcohols O—H stretching [25].

When measuring the glass slide, all the bands were in the 670–1240 cm^{-1} region. The band at 750 cm^{-1} can be assigned to the symmetric stretching of $Si\text{-}O^-$, while the $Si\text{-}O^-$ asymmetric stretching corresponds to the band at 905 cm^{-1}. The band at 1075 cm^{-1} is due to the Si-O-Si asymmetric stretching [26].

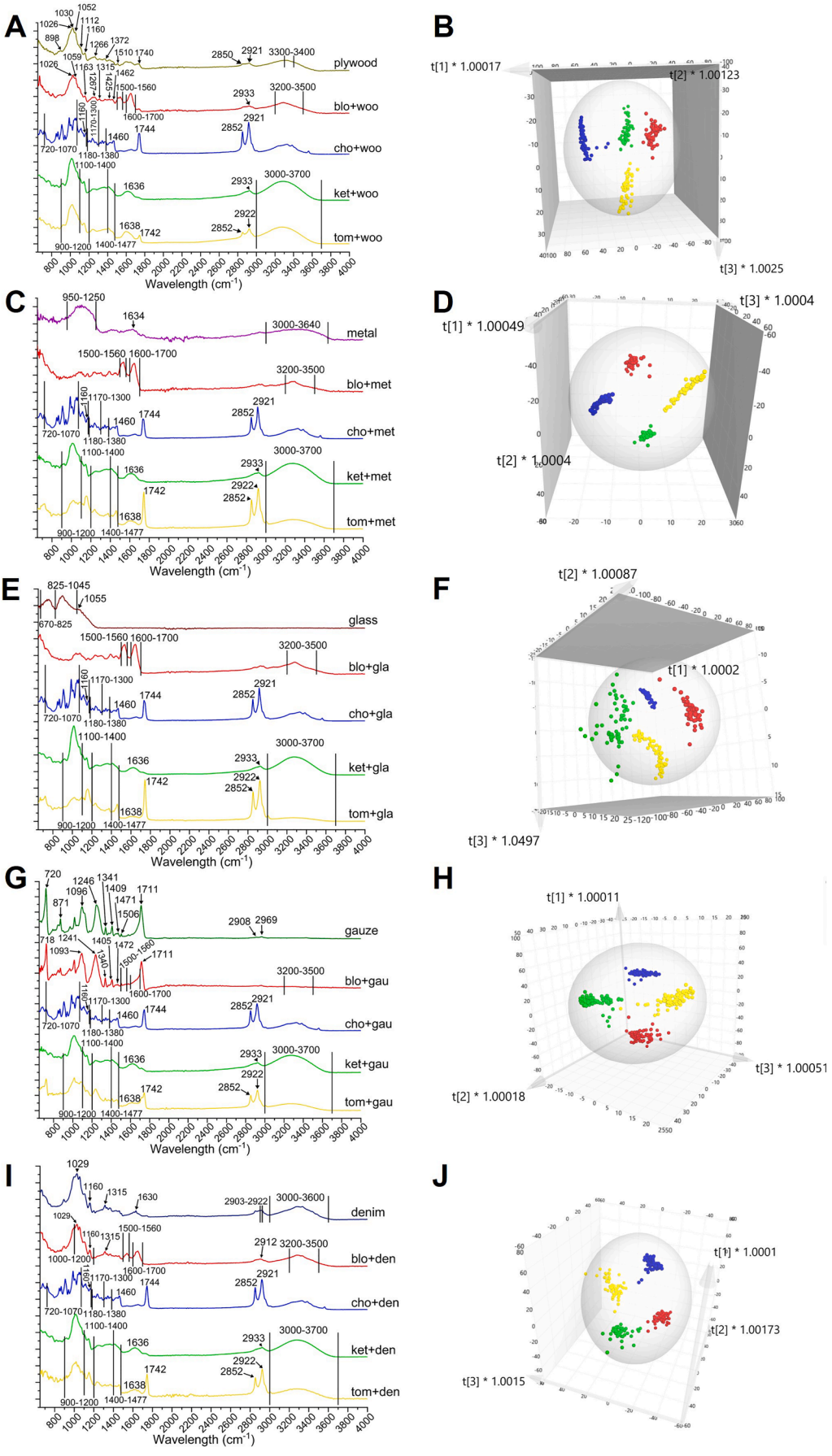

Fig. 5. A) Stack plot of the stains spectra created using plywood as a substrate, as well as of pure plywood. B) OPLS-DA 3D scatter scores plot of the model showing the separation of blood and the different interfering fluids when they formed stains on the plywood. C) Stack plot of the stains spectra created using metal as a substrate, as well as of pure metal. D) OPLS-DA 3D scatter scores plot of the model showing the separation of the different fluids when they formed stains on the metal. E) Stack plot of the stains spectra created using glass as a substrate, as well as of pure glass. F) OPLS-DA 3D scatter scores plot of the model showing the separation of the different fluids when they formed stains on the glass. G) Stack plot of the stains spectra created using gauze as a substrate, as well as of pure gauze. H) OPLS-DA 3D scatter scores plot of the model showing the separation of the different fluids when they formed stains on the gauze. I) Stack plot of the stains spectra created using denim as a substrate, as well as of pure denim. J) OPLS-DA 3D scatter scores plot of the model showing the separation of the different fluids when they formed stains on the denim. Classes: cho: chocolate (blue dots), ket: ketchup (green dots), tom: tomato (yellow dots), blo: blood (red dots).

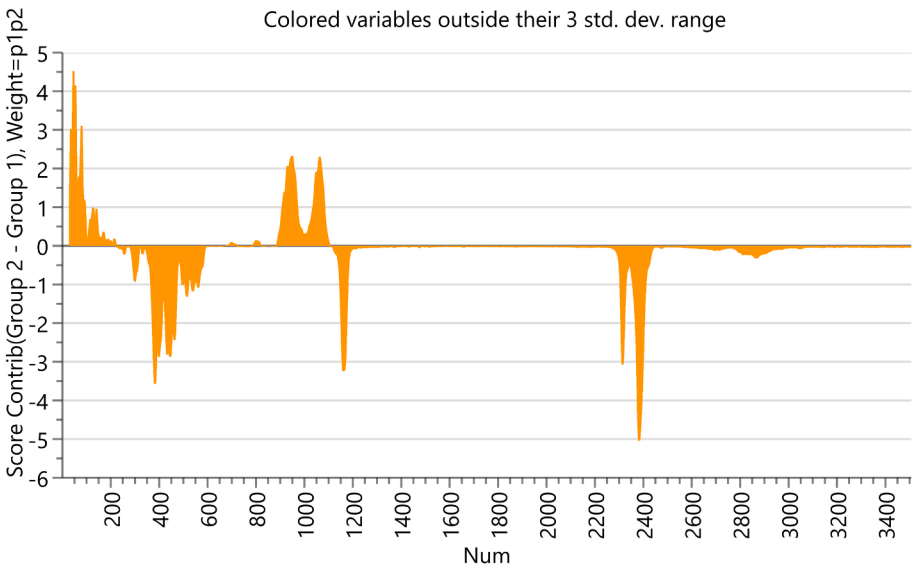

Fig. 6. Contribution plot showing the variables that differ most between the blood stains (upper part of the plot) and the interferents stains (bottom part of the plot) deposited on glass.

3.3. *Differentiation of bloodstains on different substrates*

Regardless of the substrate on which the bloodstain was analysed, the blood's Amide I (1600–1700 cm^{-1}) and Amide II (1500–1560 cm^{-1}) bands were always visible [5,12]. Fig. 4 shows the bloodstains spectra on different substrates measured by ATR FTIR. The 1000–1450 cm^{-1} region changed depending on the substrate. In the bloodstain's spectra on plywood, apart from the blood bands, some plywood characteristics bands can be seen, as described in Table 2 and Fig. 3.

The bloodstain's spectra on metal had the same bands and characteristics as the pure blood. This may be because the material is non-porous, hence the blood cannot penetrate the substrate. It accumulates on the surface, preventing any signal from the substrate from being detected.

The gauze piece is composed by polyester. The band at 1711 cm^{-1} from C═O stretching can be seen in the spectra. The band at 1241 cm^{-1} corresponds to the C—O stretching of ester groups. The one at 1093 cm^{-1} corresponds to C—O stretching [24]. Other small bands can be seen, and those are related to the substrate as can be seen in Fig. 3.

Some denim characteristic bands can be seen in the spectra. Some cellulose bands appeared in the 1000–1200 cm^{-1} region, especially the C—O stretching band at 1029 cm^{-1} and the C—O—C stretching band at 1160 cm^{-1} (Table 2). Although the 3000–3600 cm^{-1} region was dominated by the water in blood, the bands from the dye molecules N—H stretching may be located at that region too, along with the O—H stretching from the glucose alcohol groups [25].

The blood also accumulates on the glass surface because it is a non-porous material too, hence it dominates the spectrum.

Although the bloodstains spectrum is distinguishable from most of the substrates' spectra (Fig. 4), chemometrics was used to show the IR spectral differentiation in a clearer way. Therefore, an OPLS-DA model was created to discriminate the blood samples by the substrate. The blood samples on the substrates were measured fresh and then along the 28 days ageing process. All those spectra were included in the model, which had an $R^2X = 98$ % and a $Q^2 = 80$ %. Most of the bloodstains separated according to the substrate, but some samples clustered at the centre of the model. The entangled (not well discriminated) samples were measured while still fresh, whilst the samples that were separated (clustered away from the centre of the model) were measured as dry samples. Therefore, the hypothesis is that, because the blood signal is stronger in the fresh samples, they clustered according to the blood characteristics, independently of the substrate on which they were deposited. The dry samples gave a spectrum that showed both blood's and substrate's characteristics, allowing the samples to be separated according to the characteristics of the substrate they were on. To see how bloodstains are discriminated on the five substrates studied without the effect of water, a new model was made with the samples measured from 1 h up to 28 days (Figure S1). After the elimination of seven outliers, the model had an $R^2X = 98$ % and a $Q^2 = 84$ %. Figure S1 shows a good discrimination of bloodstains according to the substrate on which they are located.

3.4. *Differentiation of blood and environmental interfering stains on different substrates*

Many stains can be found at a crime scene, some of which may be bodily fluid stains relevant for the investigation, while other stains may come from irrelevant (or not) interfering substances that resemble bodily fluid stains. Hence, it is crucial for the crime investigation to correctly identify the stains, for their preservation and the information they can provide. Therefore, various blood, chocolate, ketchup, and tomato sauce stains were prepared on five different substrates and analysed by ATR FTIR assisted by OPLS-DA models. Fig. 5 shows the pure substrates' spectra together with each fluid stain's spectra on the corresponding substrate. The OPLS-DA models were calculated for differentiating the blood stains (Fig. 5). As results, in all these models, each fluid clustered separately from the others. This allowed a good differentiation of the fluids (blood and the interfering) independently of the substrate they were deposited on.

Metal, glass, and plywood are not porous materials, and therefore blood does not penetrate them. Thus, the blood or interfering stains spectra are dominant with respect to the substrates' spectra. As example, Fig. 5A shows the spectra of all studied fluids on plywood. Almost all characteristic bands of each fluid can be observed when analysed as stains on plywood. Some bands decrease in intensity, like 2852 cm^{-1} and 2921 cm^{-1} (which correspond to the polymethylene segments C—H symmetric and asymmetric stretching [17] in chocolate). However, others increase, like the 900–1200 cm^{-1} region in ketchup (which correspond to the vibrational modes of carbohydrates and acids) [18,20] (Fig. 5A). The OPLS-DA model of the fluids on the plywood surface had an $R^2X = 92$ % and a $Q^2 = 91$ % (Fig. 5B).

Fig. 5C and 5E show the fluids' spectra on metal and on glass. The stains of blood and ketchup spectra remained the same as the fluids were directly analysed on the diamond crystal. In the chocolate and tomato

sauce spectra, slight variations could be seen in some bands. The following bands were less intense when chocolate was forming a stain on metal: 1160 cm^{-1} (C—O stretching of tryacilglycerols in the liquid state), 1460 cm^{-1} (CH_2 scissoring of tryacilglycerols), 1744 cm^{-1} (C═O stretching of glycerol backbone's disordered conformational state), 2852 cm^{-1} (C—H symmetric stretching of polymethylene segments), and 2921 cm^{-1} (C—H asymmetric stretching of polymethylene segments) [17]. Similarly, the following bands from the tomato sauce also decreased their intensity when forming a stain on metal: 1742 cm^{-1} (lipids) [18], 2852 cm^{-1} (methylene C—H asymmetric stretching of lycopene), and 2922 cm^{-1} (methylene C—H symmetric stretching of lycopene) [18–20]. The OPLS-DA model using metal as a substrate (Fig. 5D) had an $R^2X = 98$ % and a $Q^2 = 93$ %. In the case of the stains on glass, the fluid's spectra were dominant, and the OPLS-DA model resulted with an $R^2X = 98$ % and a $Q^2 = 83$ % (Fig. 5F).

However, the spectra of all the fluid stains changed when they were analysed on gauze (Fig. 5G). All the peaks decreased their intensity. The spectrum that changed the least was that of ketchup, with only small changes in the 1636 cm^{-1} band (C═C stretching of olefin) [19,20]. Another OPLS-DA model was made for gauze (Fig. 5H). The model had an $R^2X = 98$ % and a $Q^2 = 94$ %.

Like the fluids' spectra on gauze, on denim, they also underwent changes with respect to their pure spectrum (Fig. 5I), since both substrates are porous materials. The spectrum that changed the most was that of the bloodstains, since new denim bands were detected in the analysis: 1029 cm^{-1} (C—O stretching of cellulose), 1160 cm^{-1} (C—O—C stretching of cellulose), and 1315 cm^{-1} (C—H wagging) [25]. Fig. 5J shows the OPLS-DA model for the denim substrate. The model had an $R^2X = 92$ % and a $Q^2 = 92$ %.

In addition, contribution or VIP plots were used to determine which of the variables has the greatest influence on the outcome of the model. As an example, Fig. 6 shows the contribution plot of the OPLS-DA model in which blood and the three interferents are differentiated when they are deposited on glass. Each bar in the contribution plot is a variable. The larger bars indicate which variables differ most among the selected groups. In the upper part of the plot are the variables that differentiate blood from the interferents, whose variables are in the bottom part of the plot. The variables that contribute most to the differentiation of blood against the interferents are in the 650–830 cm^{-1} and 1470–1680 cm^{-1} ranges, where the relevant amide bands are located. On the other side, the important variables for the interferents are in the 850–1190 cm^{-1} and 1700–1770 cm^{-1} ranges, which are related to lipids and carbohydrates, and the 2840–2950 cm^{-1} range due to the O—H from water.

The ROC plot (Figure S2) stated that the model was making a good discrimination of the four fluid samples deposited on glass. In this study, the AUC for the chocolate samples was 0.98; the AUC for the ketchup samples was 0.90; the AUC for the tomato sauce samples was 0.87, and the AUC for the blood samples was 0.91. Hence, since the AUC values were close to 1, it can be stated that the classification was quite good.

Additionally, a preliminary study of how bloodstains were discriminated by their time-since-deposition (from 1 h to 28 days) independently of the substrate, was explored by the research team [27]. An OPLS-DA model was created with the measurements of the blood stains deposited on the five different substrates (plywood, metal, glass, denim, and gauze). Interestingly, the combination of ATR FTIR with OPLS-DA showed a great potential to estimate the time-since-deposition of blood stains in a forensic context [27].

4. Conclusions and future perspectives

The correct differentiation of blood, chocolate, ketchup, and tomato sauce stains on different substrates was accomplished by ATR FTIR in the combination with OPLS-DA models. Those allowed the differentiation of the stains independently of the substrate on which they were deposited on. Using the same approach, the bloodstains could also be separated by the substrate characteristics.

These results show a proof-of-concept of how the combination of ATR FTIR with OPLS-DA differentiate bloodstains from (at least) environmental interfering stains such as chocolate, ketchup, or tomato sauce without being influenced by the substrate where they were deposited on. However, more measurements of blood samples from different donors together with varied environmental interferents (*i.e.*, different sorts of chocolate, ketchup, and tomato sauce) are needed prior its validation and reliable application in a crime scene. Thus, further investigations focused on the analysis of other bodily fluid stains and interfering substances on common substrates at crime scene, along with the analysis of bloodstains from a higher number of donors is required prior to the implementation of this analytical approach in forensic laboratories. It is also important to consider the aging process of the fluids and the analysis with other spectroscopic techniques.

CRediT authorship contribution statement

Cristina Cano-Trujillo: Formal analysis, Data curation, Investigation, Writing – original draft. **Carmen García-Ruiz:** Conceptualization, Project administration, Supervision, Writing – review & editing. **Fernando E. Ortega-Ojeda:** Data curation. **Gemma Montalvo:** Conceptualization, Project administration, Supervision, Writing – review & editing.

Declaration of Competing Interest

The authors declare that they have no known competing financial interests or personal relationships that could have appeared to influence the work reported in this paper.

Data availability

Data will be made available on request.

Acknowledgments

Authors thank Lydia Martin-Arenas for the measurement of the stains as part of her final degree project. Authors thank the funding from the European Union's Horizon 2020 research and innovation programme (SU-FCT02-2018-2019-2020) under grant agreement No 883116 (RealtIme on-site forenSic tracE qualificatioN project (RISEN). C. Cano-Trujillo thanks the University of Alcalá for her pre-doctoral grant (grant No. 572765/EXP 2022/00185).

Appendix A. Supplementary material

Supplementary data to this article can be found online at https://doi.org/10.1016/j.saa.2023.122409.

References

[1] T. Das, A. Harshey, K. Nigam, V.K. Yadav, A. Srivastava, Analytical approaches for bloodstain aging by vibrational spectroscopy: Current trends and future perspectives, Microchem. J. 158 (2020), https://doi.org/10.1016/j.microc.2020.105278.

[2] A.R. Weber, I.K. Lednev, Crime clock – Analytical studies for approximating time since deposition of bloodstains, Forensic Chem. 19 (2020), 100248, https://doi.org/10.1016/j.forc.2020.100248.

[3] R. Rosenblatt, L. Halámková, K.C. Doty, E.A.C. de Oliveira, I.K. Lednev, Raman spectroscopy for forensic bloodstain identification: Method validation vs, environmental interferences, Forensic Chem. 16 (2019), https://doi.org/10.1016/j.forc.2019.100175.

[4] R. Kumar, K. Sharma, V. Sharma, Bloodstain age estimation through infrared spectroscopy and Chemometric models, Sci. Justice. 60 (2020) 538–546, https://doi.org/10.1016/j.scijus.2020.07.004.

[5] E. Mistek-Morabito, I.K. Lednev, Discrimination of menstrual and peripheral blood traces using attenuated total reflection Fourier transform-infrared (ATR FT-IR) spectroscopy and chemometrics for forensic purposes, Anal. Bioanal. Chem. 413 (2021) 2513–2522, https://doi.org/10.1007/s00216-021-03206-w.

[6] K.M. Elkins, Rapid Presumptive Fingerprinting of Body Fluids and Materials by ATR FT-IR Spectroscopy, J. Forensic Sci. 56 (2011) 1580–1587, https://doi.org/10.1111/j.1556-4029.2011.01870.x.
[7] F. Zapata, M. Fernández-de-la-Ossa, C. García-Ruiz, Differentiation of Body Fluid Stains on Fabrics Using External Reflection Fourier Transform Infrared Spectroscopy (FT-IR) and Chemometrics, Appl. Spectrosc. 70 (2016) 654–665, https://doi.org/10.1177/0003702816631303.
[8] A.A. Quinn, K.M. Elkins, The Differentiation of Menstrual from Venous Blood and Other Body Fluids on Various Substrates Using ATR FT-IR Spectroscopy, J. Forensic Sci. 62 (2017) 197–204, https://doi.org/10.1111/1556-4029.13250.
[9] A. Takamura, K. Watanabe, T. Akutsu, H. Ikegaya, T. Ozawa, Spectral Mining for Discriminating Blood Origins in the Presence of Substrate Interference via Attenuated Total Reflection Fourier Transform Infrared Spectroscopy: Postmortem or Antemortem Blood? Anal. Chem. 89 (2017) https://doi.org/10.1021/acs.analchem.7b01756.
[10] A. Takamura, K. Watanabe, T. Akutsu, T. Ozawa, Soft and Robust Identification of Body Fluid Using Fourier Transform Infrared Spectroscopy and Chemometric Strategies for Forensic Analysis, Sci. Rep. 8 (2018) 8459–18410, https://doi.org/10.1038/s41598-018-26873-9.
[11] S. Sharma, R. Chophi, R. Singh, Forensic discrimination of menstrual blood and peripheral blood using attenuated total reflectance (ATR)-Fourier transform infrared (FT-IR) spectroscopy and chemometrics, J. Leg. Med. 134 (2020) 63–77, https://doi.org/10.1007/s00414-019-02134-w.
[12] E. Mistek-Morabito, I.K. Lednev, Discrimination between human and animal blood by attenuated total reflection Fourier transform-infrared spectroscopy, Commun. Chem. 3 (2020) 1–6, https://doi.org/10.1038/s42004-020-00424-8.
[13] A.J. Rein, J. Seelenbinder, Handheld and Portable FTIR Spectrometers for the Analysis of Materials: Taking the Lab to the Sample, Am. Lab. 45 (2013) 16.
[14] Å Rinnan, F.v.d. Berg, S.B. Engelsen, Review of the most common pre-processing techniques for near-infrared spectra, TrAC, Trends Anal. Chem. 28 (2009) 1201-1222. 10.1016/j.trac.2009.07.007.
[15] L. Eriksson, E. Johansson, N. Kettaneh-Wold, J. Trygg, C. Wikstr, S. Wold, Multi- and Megavariate Data Analysis. Part I Basic Principles and Applications. Second revised and enlarged edition, 2nd ed., Umetrics, Umeå, Sweden, 2006.
[16] M. Bylesjö, M. Rantalainen, O. Cloarec, J.K. Nicholson, E. Holmes, J. Trygg, OPLS discriminant analysis: combining the strengths of PLS-DA and SIMCA classification, J. Chemometrics. 20 (2006) 341–351, https://doi.org/10.1002/cem.1006.
[17] F. Kaneko, K. Oonishi, H. Uehara, H. Hondoh, Polarized FTIR ATR Spectroscopic Study on the Structure of Chocolate: Influence of Mold on Fat Crystalline Structures, Cryst. Growth Des. 21 (2021) 3290–3298, https://doi.org/10.1021/acs.cgd.1c00027.
[18] I.R. Bunghez, M. Raduly, S. Doncea, I. Aksahin, R.M. Ion, Lycopene determination in tomatoes by different spectral techniques (UV- VIS, FTIR and HPLC), Dig. J. Nanomater. Bios. 6 (2011) 1349–1356.
[19] M.M. Kamil, G.F. Mohamed, M.S. Shaheen, Fourier Transformer Infrared Spectroscopy for Quality Assurance of Tomato Products, J Am Sci. 7 (2011) 559–572.
[20] J. Coates, Interpretation of Infrared Spectra, A Practical Approach, John Wiley & Sons Ltd, Chichester, UK, 2000.
[21] K.K. Pandey, A study of chemical structure of soft and hardwood and wood polymers by FTIR spectroscopy, J. Appl. Polym. Sci. 71 (1999) 1969–1975, https://doi.org/10.1002/(SICI)1097-4628(19990321)71:123.0.CO;2-D.
[22] S.R. Yeomans, Galvanized Steel Reinforcement in Concrete, Elsevier Science & Technology, Oxford, 2004.
[23] .S. Fernandes, E.d.A. Alvarenga, P.R.G. Brandão, Lins, Vanessa de Freitas Cunha, Infrared-spectroscopy analysis of zinc phosphate and nickel and manganese modified zinc phosphate coatings on electrogalvanized steel, REM, Rev. Esc. Minas. 64 (2011) 45-49. 10.1590/S0370-44672011000100005.
[24] P. Peets, I. Leito, J. Pelt, S. Vahur, Identification and classification of textile fibres using ATR-FT-IR spectroscopy with chemometric methods, Spectrochim. Acta, Part A 173 (2017) 175–181, https://doi.org/10.1016/j.saa.2016.09.007.
[25] T.L. Silva, A.L. Cazetta, P.S.C. Souza, T. Zhang, T. Asefa, V.C. Almeida, Mesoporous activated carbon fibers synthesized from denim fabric waste: Efficient adsorbents for removal of textile dye from aqueous solutions, J. Cleaner Prod. 171 (2018) 482–490, https://doi.org/10.1016/j.jclepro.2017.10.034.
[26] T. Palomar, A. Chabas, D.M. Bastidas, D. de la Fuente, A. Verney-Carron, Effect of marine aerosols on the alteration of silicate glasses, J. Non Cryst. Solids. 471 (2017) 328–337, https://doi.org/10.1016/j.jnoncrysol.2017.06.013.
[27] C. Cano-Trujillo, J. Saldaña, F. E. Ortega-Ojeda, C. García-Ruiz, G. Montalvo, Application of ATR FTIR spectroscopy on tracing the aging of blood stains on substrates for forensics. https://www.thermofisher.com/es/es/home/industrial/spectroscopy-elemental-isotope-analysis/spectroscopy-elemental-isotope-analysis-learning-center/molecular-spectroscopy-information/ftir-information/ftir-applications.html, In publication.